CrossMark

MCG+07-20-052: Interacting Dwarf Pair in a Group Environment

Sanjaya Paudel[1] , Chandreyee Sengupta[2], Suk-Jin Yoon[1] , and Daya Nidhi Chhatkuli[3]
[1] Department of Astronomy and Center for Galaxy Evolution Research, Yonsei University, Seoul 03722, Republic of Korea; sjyoon0691@yonsei.ac.kr
[2] Purple Mountain Observatory, Chinese Academy of Sciences, Nanjing, 210034, People's Republic of China
[3] Central Department of Physics, Tribhuvan University, Kirtipur, Kathmandu, Nepal

Abstract

We present an observational study of the interacting pair of dwarf galaxies, MCG+07-20-052, in the vicinity of Milky Way mass spiral galaxy NGC 2998. MCG+07-20-052 is located at a sky-projected distance of 105 kpc from NGC 2998 and the two have a relative line-of-sight velocity of 60 km s^{-1}. We observed tidal tail-like extensions on both members (D1 and D2) of the interacting pair MCG+07-20-052. The interacting dwarf galaxies, D1 and D2, have B-band absolute magnitudes of −17.17 and −17.14 mag, respectively, and D2 is significantly bluer than D1. We obtained H I 21 cm line data of the NGC 2998 system using the Giant Metrewave Radio Telescope to get a more detailed view of the neutral hydrogen (H I) emission in the interacting dwarf galaxies and in the galaxy members of the NGC 2998 group. Evidence of a merger between the dwarf galaxies in the MCG+07-20-052 is also present in the H I kinematics and morphology where we find that H I is mostly concentrated around D2, which also shows a higher level of star-forming activity and a bluer $g–r$ color index compared to D1. In addition, we detect extended tenuous H I emission around another member galaxy, NGC 3006, located close to the MCG+07-20-052 pair at a sky-projected distance of 41 kpc. We compare here our results from the MCG+07-20-052 pair NGC 2998 system with other known Large Magellanic Cloud/Small Magellanic Cloud/Milky Way-type systems and discuss the possible origin of the dwarf–dwarf interaction.

1. Introduction

The theory of large-scale structure formation with Λ cold dark matter cosmology predicts that a major mass assembly of galaxies happens in a hierarchical way and in this hierarchy low-mass galaxies play a crucial role. They are, indeed, the dominant population at all redshifts and simulations predict that dwarf galaxies experience on average three major mergers in their lifetime (Fakhouri et al. 2010). While dwarf–dwarf mergers were expected to be more common in the early universe (Klimentowski et al. 2010; Fitts et al. 2018), recent observations have shown that they are also present in current epoch. The interaction between dwarf galaxies in isolated environments are frequently reported, however they are rare around a massive host (Stierwalt et al. 2015; Paudel et al. 2018a; Kado-Fong et al. 2020).

Massive galaxy mergers have been studied in great detail in both observation and numerical simulations (Barnes 1992; Naab & Ostriker 2009; Duc et al. 2011). The dwarf–dwarf interactions, on the other hand, are only starting to be explored as a population (Stierwalt et al. 2015; Pearson et al. 2016; Besla et al. 2018; Paudel et al. 2018a). This is partly because such systems are possibly not common in the local universe or they are fainter, which makes them harder to detect. The presence of tidal tails, shells, and streams have been studied in great detail around massive galaxies, which provides an unequivocal proof of merger origin of these galaxies (Duc et al. 2015). However for dwarf galaxies, such observations are few. The small shell-like feature at the Fornax dwarf galaxy detected by Coleman et al. (2004) indicated merger and recently Paudel et al. (2017) presented a detailed analysis of shell feature early-type dwarf galaxies in the Virgo cluster suggesting merger origin.

Gas-rich mergers of massive galaxies leading to the bursts of star formation play an important role in the stellar mass growth and morphological evolution (Mihos & Hernquist 1994; Wilman et al. 2013). However, the physical processes that trigger enhanced star formation activity in the low-mass galaxies are still not well understood. Often to explain starburst activity in blue compact dwarf galaxies (BCDs), similar processes of massive galaxies, e.g., the mergers and interactions, have been proposed (Noeske et al. 2001; Bekki 2008; Lee et al. 2009; Privon et al. 2017). For the Large and Small Magellanic clouds (LMC and SMC), interaction is a frequently mentioned reason in the literature to explain the enhanced star formation activity (Harris & Zaritsky 2009; Glatt et al. 2010). The LMC–SMC system is located in the group environment in vicinity of the Milky Way (MW). A number of studies have shown that such interaction in the group environment is not common and the pair can be quickly disrupted by the host tidal potential (Robotham et al. 2012; Deason et al. 2014). In this paper, we present yet another dwarf–dwarf interacting system (MCG+07-20-052), located in the vicinity of NGC 2998.

2. Interacting Dwarf

As our primary interest is to find low-mass interacting galaxies in the nearby universe, we carried out a systematic search for such objects in the local volume ($z < 0.02$). We published the most extended catalog of interacting dwarf galaxies (Paudel et al. 2018b), which comprises 177 interacting dwarf galaxies. These galaxies are selected by the visual inspection of color images of the two wide-field optical surveys (SDSS-III and the Legacy Survey). We select them according to their observed low surface brightness features that are likely the result of an interaction between dwarf galaxies. The parent sample of the dwarf galaxies is selected from NASA Extragalactic Database (NED) with a magnitude cut of $M_r > -19$ mag. We found that a significant majority of

interacting dwarfs are located in the isolated environment and less then 10% of them are located in the vicinity of giant, MW mass, or more massive galaxies. Recently, Kado-Fong et al. (2020) also published a sample of interacting dwarf galaxies where they study the star formation and host properties. They also found that dwarf galaxies that host tidal debris are systematically blue, indicating merger-induced star formation, which agrees with the findings of Paudel et al. (2018b) where an overwhelming majority of interacting dwarf galaxies are star forming and blue.

To maximize the number of systems where the interacting galaxies are in spatial and kinematic proximity similar to the LMC–SMC–MW, we defined an LMC–SMC–MW analog as the interacting dwarf located within a 300 kpc sky-projected distance from the MW mass galaxy with a relative line-of-sight velocity less than 300 km s^{-1}. Indeed this simple criteria does not entirely reflect the actual LMC–SMC orbital and spatial properties. LMC and SMC are located relatively close, <60 kpc, to the MW compared to our 300 kpc projected distance of an interacting dwarf from the host. One of the main motivations for using this criteria is that we do not have three-dimensional information of our system whereas in the case of LMC and SMC, we know their detailed spatial and orbital information in six dimensions.

Among the LMC–SMC–MW analogs found using our criteria, we selected a few systems to study further in detail with H I 21 cm observations. MCG+07-20-052 is the second object in this series. Previously, we studied the UGC 4703 interacting pair near the isolated spiral NGC 2718 (Paudel & Sengupta 2017), where we discussed the similarity of UGC 4703 pair galaxies to the LMC–SMC system.

2.1. MCG+07-20-052

MCG+07-20 is located at the sky position of R.A. = 09:49:06.46, decl. = +44:02:54.35 and a redshift of z = 0.01575. It is an interacting pair of star-forming dwarf galaxies located in a group environment. The most massive galaxy in the group, NGC 2998, is an MW mass spiral. The NGC 2998 group is a relatively dense group that has at least seven member galaxies of stellar mass larger than $10^8 M_\odot$ within the 300 kpc sky-projected radius and relative line-of-sight radial velocity ±300 km s^{-1} from the central galaxy. NGC 2998. MCG+07-20-052 is the nearest neighbor to the spiral galaxy NGC2998 at a sky-projected distance of 105 kpc[4] and they have a relative line-of-sight radial velocity of 60 km s^{-1}.

3. Data Analysis

3.1. Analysis of Archival Data

Optical band photometric measurements were done in the archival images available at the Sloan Digital Sky Survey (SDSS)-III Data Archive Server (Abazajian et al. 2009). Although deeper optical images are also available from the Legacy survey (Blum et al. 2016), we did not use them for the photometric measurement because their flux calibration and sky-background subtraction are not as good as the SDSS images. In this paper, we used the Legacy survey images only for display purpose. The SDSS images were already bias-subtracted, flat-field-corrected, sky-subtracted, and flux-

calibrated. We used a tool provided by the SDSS-III to create a mosaic image with a large field of view and no further effort has been made on the image reduction part. However, we used a simple and similar approach to subtract the sky-background count as in our previous publications (Paudel et al. 2018b, 2018a).

In Figure 1, we show the Legacy $g-r-z$ combined tri-color image with a field of view of $14' \times 15'$ around NGC 2998 that covers all member galaxies of the group. MCG+07-20-052 is located in between the NGC 3006 and NGC 2998 and two tidal tail-like extensions can be seen emanating from the interacting dwarf pair along the direction of NGC 2998. The sky-projected separation between NGC 3006 and MCG+07-20-052 is 41 kpc and the relative line-of-sight velocity between the two is 100 km s^{-1}. The relative line-of-sight velocities of D1 and D2 from NGC 2998 are 18 and 59 km s^{-1}, respectively.

In Figure 2, we show a zoomed-in region around MCG+07-20-052 and NGC 3006. We named the two interacting dwarf galaxies in MCG+07-20-052 pair as D1 and D2 located to the east and west respectively. Their sky-projected separation is 7.5 kpc, which we measured calculating the centroid of each individual, see the cross marks at Figure 2. Although both galaxies look like typical blue star-forming galaxies, the observed color distribution shows that the main body of D1 is slightly redder and smooth. On the other hand, the main body of D2 is clumpy and its morphology mimics a typical tadpole galaxy with a prominently blue star-forming head and a low surface brightness tail (Elmegreen et al. 2012). A careful look at NGC 3006 reveals a low surface brightness (slightly above the detection limit) extension toward MCG+07-20-052, which is significantly blue compared to the main body of the galaxy. The region has been marked with a dashed line in Figure 2.

To measure the photometric parameters of each individual galaxy, we performed aperture photometry in the SDSS g- and r−band filter images. We chose different aperture sizes for each individual galaxy depending on their extension, but kept them fixed for different filters. The sizes of apertures were selected visually and they were wide enough to secure all the flux in the region of interest. Before the doing aperture photometry, we masked all unrelated foreground and background objects manually. Foreground Galactic extinction correction was done by applying an extinction map of Schlafly & Finkbeiner (2011) and no correction has been made for internal extinction and cosmological deeming, the later being actually insignificant.

The result of the photometric measurements are listed in Table 1. We converted the SDSS g-band magnitudes to B-band magnitudes using an equation, $B = g + 0.227 \times (g - r) - 0.337$, provided by the SDSS color transformation tool.[5] To derive the stellar mass, we used the r−band magnitude with an appropriate mass-to-light ratio (M/L). The M/L is obtained using $\log(M/L) = -0.306 + 1.097 \times (g - r)$. This assumes a simple stellar population with a single burst of star formation to derive a relation between the mass-to-light ratio and galaxy color. Indeed, galaxy star formation histories are complex. However, it is shown that scatter in the mass-to-light ratio derived from different star formation history for a given color is ∼0.2 dex, see Section 4.3 of Zhang et al. (2017). Therefore, we consider ±0.2 dex as a typical conservative error on our stellar mass estimates.

---

[4] We use an NED quoted distance of 60 Mpc for the NGC 2998 group. The distance is derived from the Tully–Fisher relation (Tully et al. 2016).

[5] http://www.sdss3.org/dr8/algorithms/sdssUBVRITransform.php
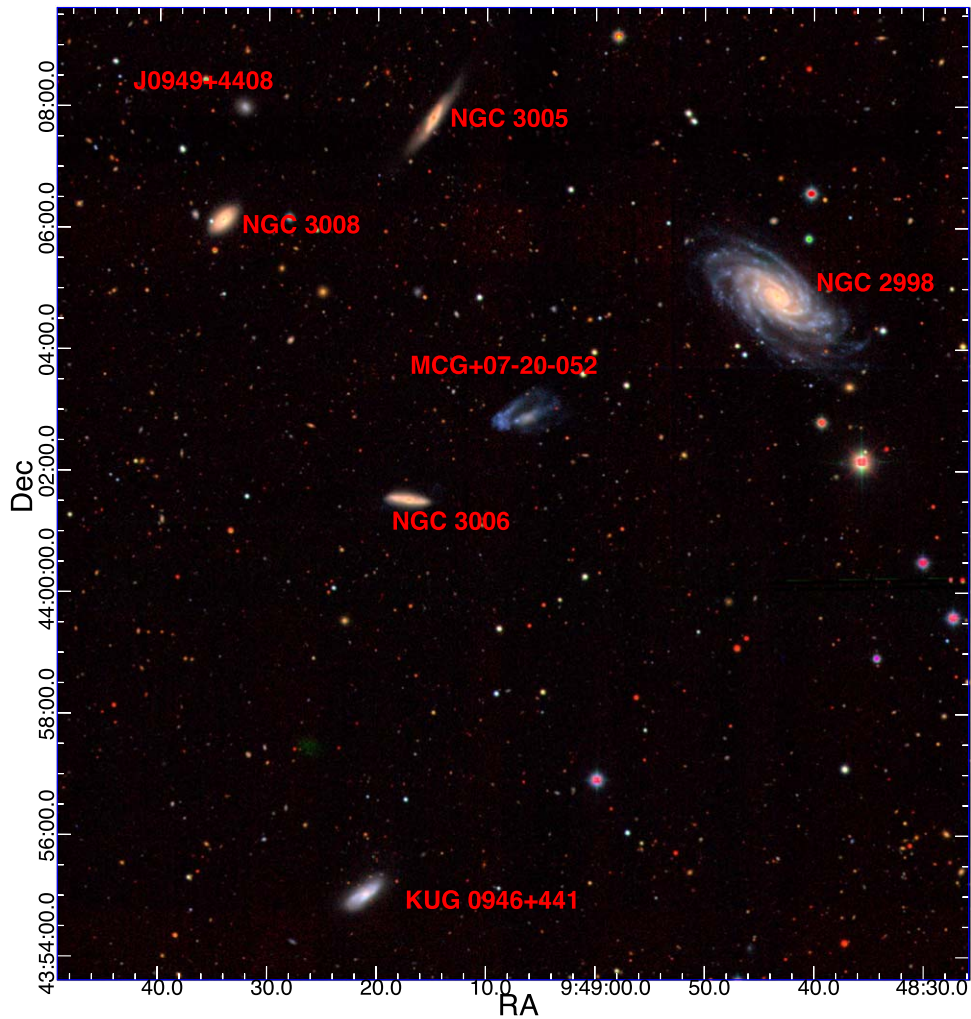
Figure 1. Optical view NGC 2998 seen from the SDSS $g-r-z$ combined tri-color image. The field of view is $14' \times 15'$. The center is adjusted to include all galaxies in the field of view and they are marked.

The interacting dwarfs, D1 and D2, have a similar brightness with B-band absolute magnitudes of -17.17 and -17.14 mag, respectively, but D2 is significantly bluer. Their $g - r$ color indexes are 0.23 and 0.05 mag, respectively. Overall, a combined (D1+D2, a.k.a, MCG+07-20-052) photometry, with a large aperture that covers both, yields a B-band absolute magnitude of -17.94 mag. NGC 3006 has a B-band absolute magnitude of -18.28 mag and it turns out much redder than an interacting dwarf pair with a $g - r$ color index of 0.66 mag. The estimated stellar mass of D1, D2, and NGC 3006 are 5.37×10^8, 2.63×10^8, and 8.12×10^9 $M_\odot$, respectively. That gives a stellar mass ratio between the interacting dwarfs pair of $\sim$2:1.

We measured the $g - r$ color index of the tidal tail-like extensions of D1 and D2, marked with the dashed line in Figure 2. We found the tidal tails of both the dwarfs to have a similar $g - r$ color index of 0.22 mag. And for NGC 3006, we found the low surface brightness eastern extension, also marked with a dashed line in Figure 2, to be significantly bluer compared to its main body, with a $g - r$ color index of 0.14 mag.

To calculate ongoing star formation rates we used the *Galaxy Evolutionary Explorer* (*GALEX*) images. The area around NGC 2998 is covered by the *GALEX* all-sky survey (Martin et al. 2005) and we downloaded the intensity map from the archive. Although the all-sky survey images are not of deep exposure, we still find a reasonable detection in far-UV (FUV) band images for all galaxies in the NGC 2998 system. We performed aperture photometry as done in the SDSS images in both FUV images. We derived the star formation rates from the FUV flux using a calibration provided by Kennicutt (1998). The values are listed in Table 1.

The SDSS fiber spectroscopy has targeted the brighter galaxy, D1, of the interacting pair and its measured optical redshift is $z = 0.0156$. We obtain the optical spectrum from the SDSS archives. The SDSS $3''$ diameter fiber is placed at a relatively red part of central body and the spectrum continuum does not have a high S/N. However, the emissions from early Balmer lines (Hα, Hδ, Hγ, and Hβ) are clear. The Hα equivalent width measured in the SDSS fiber spectrum is 15 Å and this value is not high enough to consider the galaxy as a starburst, which is typical for local blue compact dwarf galaxies (BCDs; Meyer et al. 2014). Emission line metallicity derived
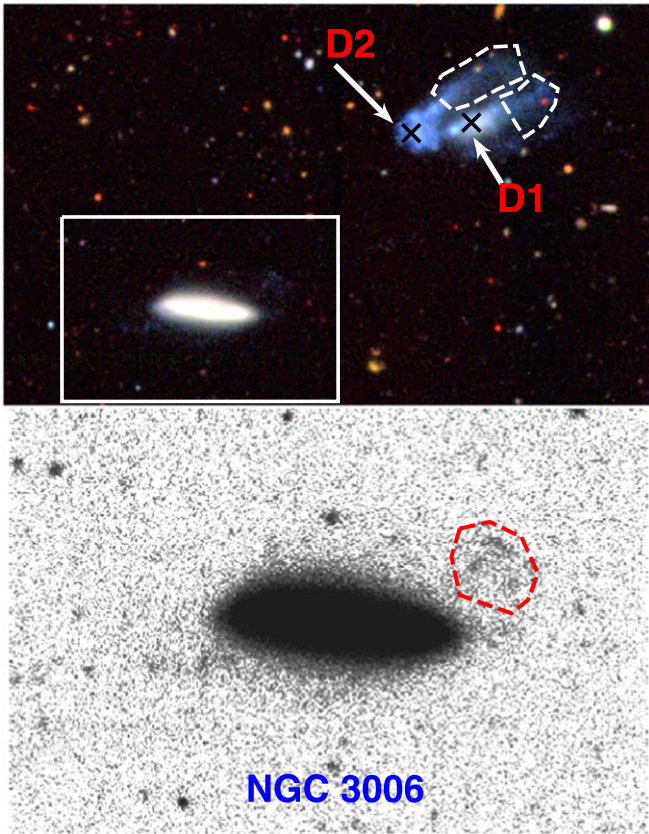
Figure 2. Zoomed-in view of the region around MCG+07-20-052 and NGC 3006. The upper panel image is reproduced same way as Figure 1, which has a field of view of $4.'5 \times 3'$. Here we marked the two interacting dwarf galaxies (D1 and D2) in MCG+07-20-052. The supposed center, calculated as the centroid, of D1 and D2 are also marked by black crosses and their separation is $25.''77$. In lower panel image, we show further zoom-in of NGC 3006 and this image is reproduced by co-adding legacy $g-r-z$ band images to gain signal at the low surface regions. The polygons, white in top panel and red in the lower panel, represent the regions of stellar stream we have chosen for the photometric measurement, see the text.

from a ration of $H\alpha/[N\,II]$ is 8.2 (Marino et al. 2013) and the star formation rate derived from the $H\alpha$ emission line flux is 0.001 $M_\odot\,yr^{-1}$, which is significantly lower than the star formation rate derived from the FUV flux. However we note that $3''$ diameter fiber spectroscopy only represents the central part of the galaxy and the star formation rate derived from the FUV flux is summed over the entire galaxy.

3.2. H I 21 cm Observations

H I observations of MCG+07-20-052 were carried out using the Giant Metrewave Radio Telescope (GMRT[6]) located at Pune, India. The system was observed between 2019 January 30 and February 1 as a part of our observing proposal "GMRT H I mapping of LMC–SMC–MW analog." A 16 MHz bandwidth was used yielding a velocity resolution of $\sim 7\,km\,s^{-1}$. The GMRT primary beam at the L band is $24'$ and the synthesized beams of the images presented in the paper are $37.''0 \times 32.''9$ (low resolution) and $15.''3 \times 11.''9$ (high resolution). At the adopted distance of MCG+07-20-052, 60 Mpc, $37''$, and $15''$ sample 11 kpc and 4 kpc respectively. The data was analyzed using the software AIPS.[7] After flagging bad data for radio

---

[6] http://www.ncra.tifr.res.in/ncra/gmrt
[7] http://www.aips.nrao.edu

frequency interference or from malfunctioning antennas, the UV data was calibrated and continuum subtracted. Image cubes of various resolutions were then made using the AIPS task IMAGR. Finally the integrated H I, velocity field, and velocity dispersion maps were made from the H I cubes using the AIPS task MOMNT. Further details of the observations are given in Table 2.

Figure 3 shows a low-resolution integrated H I map overlaid on the SDSS $g-r-z$ co-added image. Significant H I emission is detected in four galaxies NGC 2998, MCG+07-20-052, NGC 3006, and KUG 0946+441. NGC 3005 and NGC 3008 show marginal detections. The H I masses of the interacting dwarf pair MCG+07-20-052 and its two significant neighbors, NGC 3006 and NGC 2998, were estimated from our observations and are listed in Table 1. Lack of spatial resolution limited us from estimating individual masses of D1 and D2. The H I disk in NGC 2998 seem quite regular and unperturbed while both MCG+07-20-052 and NGC 3006 show extended and irregular H I morphologies. The high-resolution ($15.''3 \times 11.''9$) image of a part of the field, with NGC 3006 and MCG+07-20-052, is presented in the inbox. The outermost contour here is $\sim 2.5 \times 10^{20}\,cm^{-2}$ compared to the outermost contour of $0.4 \times 10^{20}\,cm^{-2}$ tracing the diffuse gas in the low-resolution image. In MCG+07-20-052, the high-resolution image reveals that the H I peaks in the merger system coincide mostly with D2. While it was not possible to resolve emission from individual galaxies, two H I peaks were detected. The stronger peak coincides with the head of the tadpole D2, and the other one is seen in the region between D1 and D2, see the inset of Figure 3. The H I distribution in NGC 3006 is extended significantly beyond the optical size of the galaxy. The H I disk of NGC 3006 is almost U-shaped and extends toward MCG+07-20-052, though no H I bridge was detected between NGC 3006 and MCG+07-20-052.

Figure 4 shows the H I velocity field of NGC 2998, the MCG +07-20-052 pair, and NGC 3006. In top panel, we show the velocity field obtained from the low-resolution H I cube. In bottom panel, we show a zoomed-in view of the region highlighted by a green box in the top panel and it shows the high-resolution velocity field. As seen in the low-resolution image, NGC 2998 does not seem to be kinematically affected by any of the other galaxies. H I in the MCG+07-20-052 seem to be merged with the bulk of the gas shifted toward D2. We see no signs of rotation or clear velocity gradient in D1 and D2 and they are indistinguishable even in the high-resolution image. The velocity field of NGC 3006 seems to be preserving its rotation while showing an extended U-shaped morphology, an asymmetry possibly caused by some past interactions. The gas kinematic center seems to be coincident with the optical center. The H I spectrum of NGC 3006 shows a regular rotating feature as we can see the classic double-horn profile and its center perfectly matches with the optical velocity of the galaxy center, Figure 5 blue line. SDSS spectroscopy exists for two pointings in NGC 3006: one at the center and another to its west, which have been marked by the black crosses. We find that the gradient in the optical velocity of NGC 3006 matches with that of the H I velocity, suggesting that the gas and stellar masses share the same sense of rotation. However, we note that the spatial resolution of our observations, specially the H I data, is not sufficient to make strong claims about the matching gradient, nonetheless the matching spectral line width combined with the velocity gradient information from the optical and H I maps suggest an alignment of gas and stellar kinematics in NGC 3006.

Table 1
Physical Properties Galaxies in the NGC 2998 System

Galaxy	R.A. (deg)	Decl. (deg)	z	M_B (mag)	$g-r$ (mag)	D (kpc)	SFR $\log(M_\odot\,yr^{-1})$	M_* $\log(M_\odot)$	$M_{H\,I}$ $\log(M_\odot)$
NGC 2998	147.1825	44.0815	0.01595	−20.94	0.43	000	0.39	10.58	10.67
NGC 3006	147.3221	44.0259	0.01600	−18.28	0.66	152	−1.03	9.91	9.43
NGC 3005	147.3125	44.1313	0.01515	−17.99	0.75	141	−1.49	9.95	
NGC 3008	147.3927	44.1026	0.01579	−18.65	0.75	214	−1.66	10.21	
KUG 0946+441	147.3383	43.9179	0.01585	−18.68	0.33	228	−0.86	9.51	
J0949+4408	147.3849	44.1338	0.01512	−16.18	0.37	212	−1.29	8.58	
D1	147.2771	44.0483	0.01575	−17.17	0.23	101	−0.78	8.73	
D2	147.2870	44.0470		−17.14	0.05	111	−0.66	8.42	
MCG+07-20-052				−17.94	0.18	105	−0.40	8.96	9.18

Note. We list the galaxies names and their position in sky (RA & Dec) in columns 1–3, respectively. In the last row MCG+07-20-052 represents a combined value of D1 and D2. The listed redshifts, in the fourth column, are obtained from the SDSS spectroscopy. The B-band magnitudes, in the fifth column, are converted from the g-band magnitudes and corrected for foreground Galactic extinction. A typical error on the magnitudes is 0.01 mag in all optical band photometry. The star formation rates are derived from FUV flux measured in the *GALEX* all-sky survey images. The stellar mass, listed in column 8, is derived from the SDSS r–band magnitudes in which we expect a systematic uncertainty of 0.2 dex, see the text.

Table 2
GMRT Observation Details

Frequency	1398.3949 MHz
Observation date	2019, 30 Jan–1 Feb
Phase calibrator (flux density)	0834+555
Observation time	15.0 hr
Primary beam	24″ at 1420 MHz
Low-resolution beam	37″0 × 32″9 (PA = −12°3)
High-resolution beam	15″3 × 11″9 (PA = 20°3)
rms for low-resolution map	1.1 mJy beam^{-1}
rms for high-resolution map	0.9 mJy beam^{-1}
R.A. (pointing center)	09^h 49^m 07^{s}6
decl. (pointing center)	44^d 02^m 52^{s}0

This probably indicates that NGC 3006 has not undergone a strong interaction with any of its neighbors. Being in the group, interactions with its neighbors may have affected the outer edges of its H I disk, but they were never strong enough to disrupt its gas disk or disturb its rotation pattern. Additionally, while the H I in NGC 3006 is asymmetric and somewhat shows an extension toward MCG+07-20-052, in the velocity space they seem to be separated by ∼100 km s^{-1}, suggesting that they might have suffered a fast and weak interaction in the recent past.

4. Discussion

4.1. Comparison with the LMC–SMC–MW System and Interaction

The ongoing interaction between the LMC and SMC, indeed, is happening in a group environment in the vicinity of the MW, although a satellite pair of LMC–SMC mass around the MW mass host is not commonly seen (Robotham et al. 2012). Cosmological volume numerical simulations predict that there is less than a 10% chance that the MW mass halo would host two subhalos of the mass of the Magellanic clouds (Boylan-Kolchin et al. 2010; Tollerud et al. 2011). Similarly, analyzing the Galaxy And Mass Assembly Catalog of Galaxies, Robotham et al. (2012) estimated the probability of such systems is less than 5%. Following these statistics, the merger probability of LMC–SMC morphology dwarf galaxy satellites around the MW mass host maybe even smaller. While

analyzing the statistics, we have found ≈10% (19 out of 177) of interacting dwarfs are located within the 700 kpc sky-projected radius from the MW mass halo and among them only four are qualified as LMC–SMC–MW analogs located within the 300 kpc radius. Different authors have used different criteria to search the LMC–SMC analog. Robotham et al. (2012) selected a pair of dwarf galaxies located within the spatial and velocity radius of 100 kpc ± 400 km s^{-1}, respectively, from the host and Liu et al. (2011) selected a pair of dwarf galaxies located within the spatial and velocity radius of 100 kpc ± 300 km s^{-1}, respectively, from the host. Whereas, we selected the interacting dwarfs, not simply a pair, located within the 300 kpc sky-projected radius and ±300 km s^{-1} line-of-sight radial velocity from the host. Given different selection criteria for LMC–SMC analogs in the literature and this study, we refrain from making any strong claims and only present a qualitative comparison.

MCG+07-20-052 is located at a sky-projected distance of 105 kpc from NGC 2998, which has a stellar mass similar to the MW. We list a direct comparison of physical parameters between the LMC–SMC–MW system and the NGC 2998-MCG+07-20-052 in Table 3. In comparison to the MW and NGC 2718, NGC 2998 is located in a relatively dense environment where we find several bright (brighter than SMC) galaxies around it. There are at least seven galaxies with confirmed redshift information within a sky-projected radius of 300 kpc around NGC 2998. In addition to the galaxies presented in Figure 1, we find that NGC 3009 is located at a sky-projected distance of 442 kpc, which is a magnitude fainter than NGC 2998.

In Figure 6, we show the immediate environment of NGC 2998 within an area of ±500 kpc in the sky. The position and radial velocities of the galaxies are obtained from NED. We can see many galaxies within our selected sky area and this certainly makes the immediate environment of NGC 3009 significantly different from the MW and NGC 2718. There are only two bright star-forming galaxies located around the MW (LMC and SMC) and NGC 2718 (UGC 4703 and UGC 4703B). This, indeed, shows that NGC 2998 is located in a significantly denser environment than the MW and NGC 2718.

In NGC 2718, the interacting satellites were connected through a stellar stream where we identified a blue star-forming region, a possible candidate of the tidal dwarf galaxy
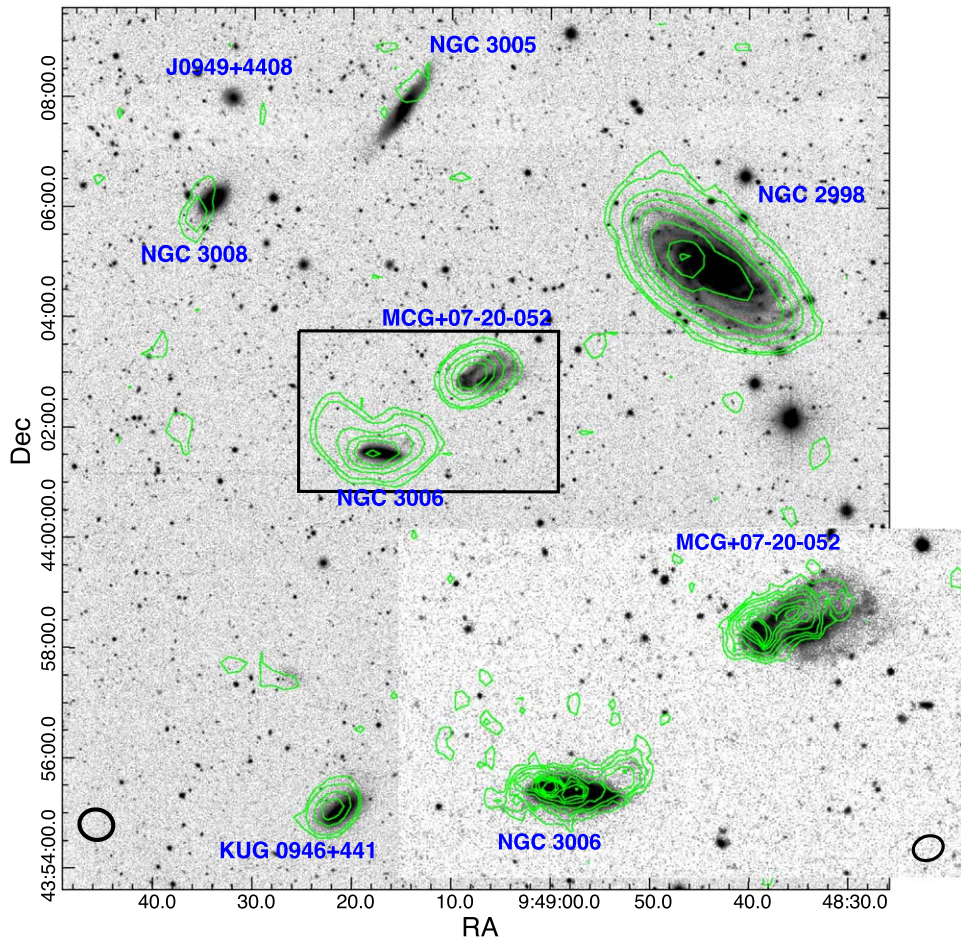
Figure 3. Integrated H I contours from the GMRT low-resolution map overlaid on the Legacy co-added g–r–z band images. The field of view of the image is similar to that in Figure 1. The H I column density levels are N(H I) $= 10^{20} \times$ (0.4, 0.9, 2.7, 4.5, 6.3, 9.0, 11.7, 13.5) cm^{-2}. A black ellipse at the bottom left corner represents beam size of the GMRT observation. In the inset we show a zoomed-in view of a region highlighted by black box with a field of view similar to Figure 2. The overlaid H I contour is obtained from a high-resolution map that has a beam size of $15''.3 \times 11''.9$, see the bottom right corner. The H I column density levels are N(H I) $= 10^{20} \times$ (2.5, 4.3, 6.1, 9.0, 12.0, 13.9, 15.1, 16.3, 18.1) cm^{-2}.

and their sky-projected separation was 20 kpc. However in MCG+07-20-052 we do not find such a stellar stream connecting the interacting dwarfs D1 and D2, and also their separation is quite small, almost overlapping each other. The lack of spatial resolution prevented us from estimating the gas loss in terms of individual H I deficiencies for D1 or D2, but we do notice a hint of an H I shift toward D2. So we tried to estimate the average gas content of the MCG pair, although we acknowledge the uncertainties are large in such an estimate. Assuming that the net H I content of $1.6 \times 10^9\ M_\odot$ is shared equally by D1 and D2, and the average optical diameter of the galaxies is $0'.5$ (8.8 kpc), the H I surface density $(M_{\mathrm{H\,I}}/D_l^2)$ value turns out to be ~ 7.0. Comparing this with the average H I surface density value of an unperturbed field galaxy of similar morphological type and taking into account the uncertainty on that number (Haynes & Giovanelli 1984), we conclude that the MCG pair shows no significant H I deficiency. Compared to the reported cases of gas transfer to the outskirts in forms of extended tails in dwarf–dwarf pairs (Pearson et al. 2016), the MCG pair shows no major gas loss and seems to retain the majority of its gas close to its optical extent. The two dwarfs D1 and D2 seem to be interacting, leading to gas transfer or a projected shift of the bulk of the gas from D1 to D2, but there

seems to be no massive gas loss from the pair into the intergalactic medium.

Our H I data is fairly deep, with the lowest H I contour tracing $\sim 4 \times 10^{19}$ cm^{-2}. But unlike the Magellanic Stream (MS) we do not detect any H I extension/emission connecting NGC 2998 and the MCG+07-20-052. Instead, we find that the H I distribution around NGC 3006, another LMC mass dwarf galaxy, to be asymmetric and stretched toward MCG+07-20-052. The warped but unperturbed rotation pattern of NGC 3006, as observed in the H I as well as optical data, suggests it may be undergoing or may have undergone a flyby interaction with its neighbor galaxy MCG+07-20-052. We derive a tidal index, Θ,[8] on the MCG+07-20-052 pair from the NGC 2998 and NGC 3006, i.e., $\Theta_{\mathrm{NGC\,2998}} \sim 2.4$ and $\Theta_{\mathrm{NGC\,3006}} \sim 3.07$. Which, indeed, shows that the tidal influence of NGC 3006 is significantly larger than that of NGC 2998. The LMC/SMC tidal index is significantly larger than these values, which is 3.7 (Pearson et al. 2016).

The head–tail elongation seen in the optical in D1 and D2 as well as the pushed U-shaped H I morphology seen in

---

[8] $\Theta = \log\left(\frac{M_*[\times 10^{11}]}{D_{\mathrm{proj}}^3}\right)$ where M_* is the stellar mass of host and D_{proj} is the projected distance from the dwarf (Karachentsev et al. 2013).
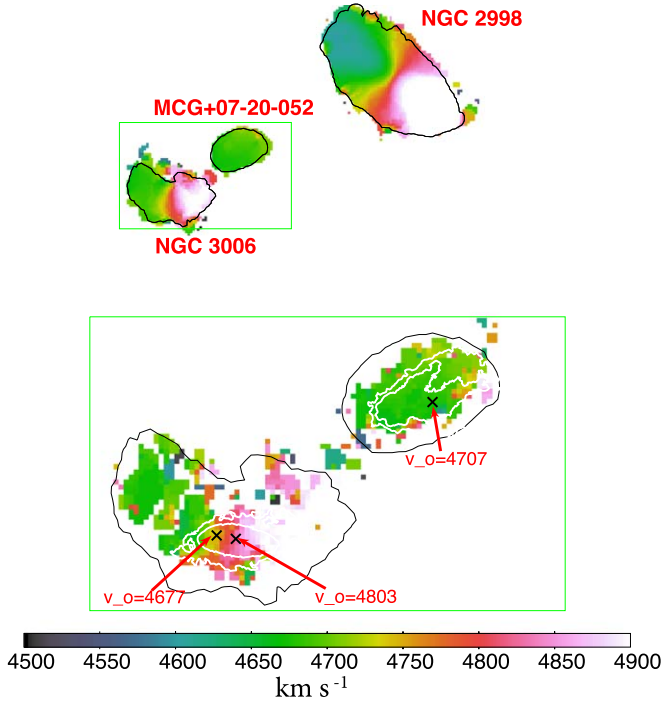
Figure 4. Top: the H I velocity field from the GMRT low-resolution cube. The black contour traces the lowest column density contour of the low-resolution integrated H I image ($N(\text{H I}) = 0.4 \times 10^{20}\,\text{cm}^{-2}$). Bottom: we show a zoomed-in view of the region highlighted by a green box. This shows the high-resolution velocity field. The white contours trace the optical g-band light at the surface brightness levels of 25 and 26.5 mag arsec^{-2} for the inner and outer, respectively. The black contour traces the lowest column density contour of the low-resolution integrated H I image, same as the top panel. The black crosses represent the SDSS fiber spectroscopy targeted position, where optical velocities are available.
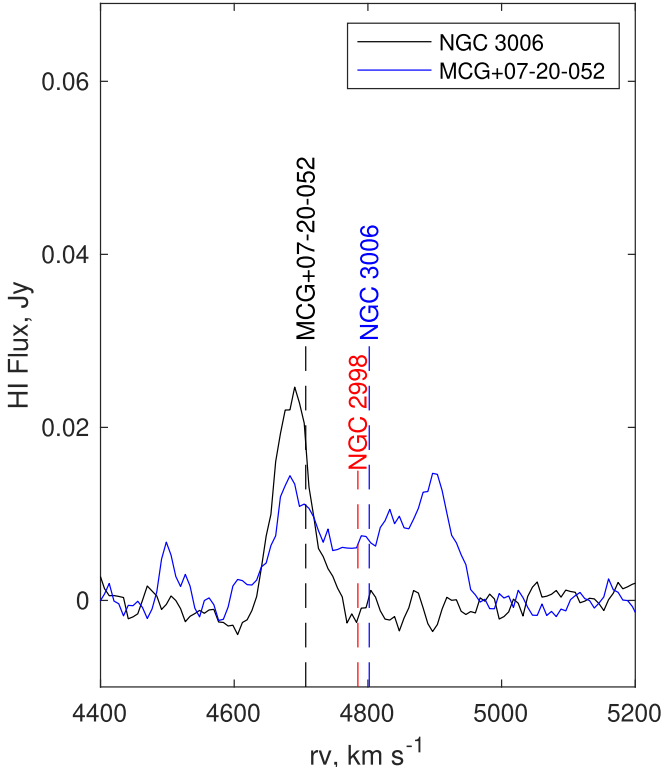
Figure 5. Integrated H I spectrum of MCG+07-20-052 and NGC 3006. To show the optical velocities, we draw a vertical dashed line for each galaxy.
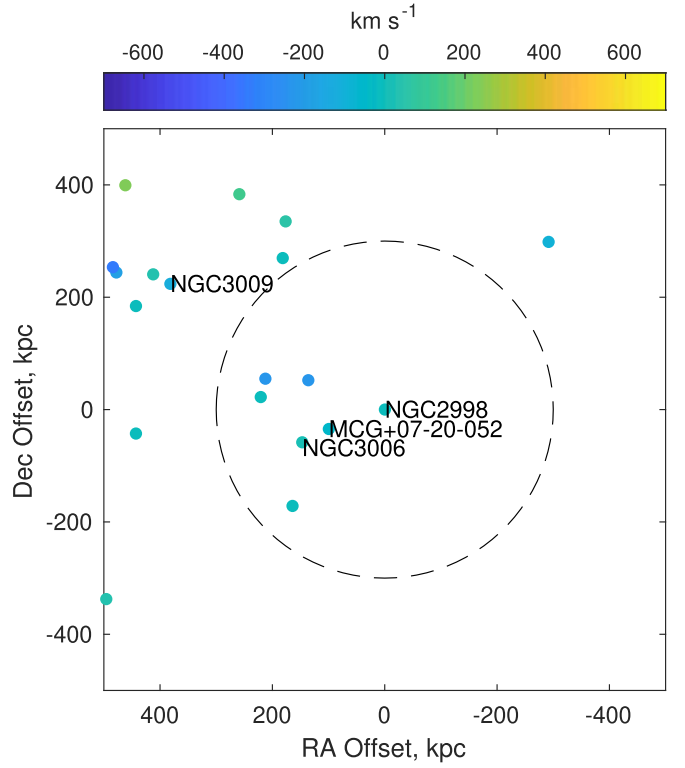
Figure 6. Distribution of galaxies around NGC 2998 where we sampled all galaxies available at the NED within the velocity range of ± 700 km s^{-1} with respect to the line-of-sight velocity of NGC 2998. The x-axis and y-axis are offsets in R.A. and decl. from NGC 2998, respectively, and both are in units of kiloparsecs. The symbol color represents their relative line-of-sight velocities with respect to NGC 2998, according to the color bar at the top of the plot. We highlight the immediate, 300 kpc sky-projected radius region around the NGC 2998 by a dotted red circle.

Table 3
Comparison with LMC–SMC, UGC470, and MCG+07-20-052

Galaxy	M_B (mag)	D (kpc)	M_* $M_\odot$	SFR $M_\odot$ yr^{-1}	H I$_{\text{mass}}$ $M_\odot$
			MW		
MW	−21.17	0	5×10^{10}	0.68–1.45	8×10^9
LMC	−18.60	50	2.3×10^9	0.2	4.4×10^8
SMC	−17.20	60	5.3×10^8	0.04	4×10^8
			NGC 2718		
NGC 2718	−21.01	0	7×10^{10}	0.97	1.12×10^{10}
UGC 4703	−18.0	81	1.8×10^9	0.2	1.4×10^{9a}
UGC 4703B	−16.5	104	5.4×10^8	0.03	
			NGC 2998		
NGC 2998	−20.94	0	3.8×10^{10}	2.45	8.7×10^9
D1	−17.17	105	5.3×10^8	0.16	1.5×10^{9a}
D2	−17.14	112	2.6×10^8	0.21	
NGC 3006	−18.28	157	8.1×10^9	0.09	2.6×10^9

Notes. The H I masses of the NGC 2998 system have been estimated from the GMRT spectra. The table is reproduced from our previous study on UGC470 in the NGC 2718 group (Paudel et al. 2018b).
[a] Combined H I mass of the interacting pair.

NGC 3006 could usually be seen as signs of ongoing ram pressure stripping (RPS; Abramson et al. 2011) in the group. Commonly known as jelly-fish galaxies, ongoing RPS galaxies

also show compression of H I on the opposite side of an elongated tail and depending on the strength of the ram pressure, the H I distribution show signs of outer edge gas stripping, e.g., JO206 (see Ramatsoku et al. 2019). Also RPS mainly affects the gas distribution before it affects the stellar disk. In MCG +07-20-052, while the tadpole-like feature is visible in the optical, we find no hint of compression or shrinking of the H I disk and the H I distribution is more extended than the galaxy's stellar distribution in both NGC 3006 and MCG+07-20-052 (see the white contour in Figure 4). Therefore this extended, merged, and asymmetric H I distribution in MCG +07-20-052 suggests that the observed tidal features on both H I gas and stellar population, including the tadpole-like appearance of the dwarfs, may have originated mainly from tidal interaction and not from RPS. Ram pressure alone could not be responsible for the optical features of D1 and D2, rather it could be tidal assisted ram pressure which is more commonly found to influence galaxy evolution in group environments (Davis et al. 1997; Sengupta et al. 2007; Besla et al. 2012; Pearson et al. 2018). In contrast, in the LMC the presence of stars well beyond the H I distribution in the leading edge suggests that RPS played a strong role and Salem et al. (2015) concludes that the disk of the LMC was truncated by the peak ram pressure at pericentric passage.

5. Conclusions

We present GMRT H I images and optical photometry data of the galaxies in the NGC 2998 group. From the data analysis and their discussion in the broader context, we draw the following conclusions.

(1) We identify MCG+07-20-052, a pair of dwarf galaxies of LMC–SMC mass, located in the vicinity of MW mass spiral galaxy NGC 2998.
(2) H I is mostly concentrated around only one member of the interacting pair, i.e., D2, which also shows a higher level of star-forming activity and bluer $g-r$ color index compared to the other member of interacting pair, i.e., D1.
(3) We detect extended tenuous emission of H I around another member galaxy, NGC 3006, located close to the MCG+07-20-052 at a sky-projected distance of 41 kpc.
(4) We present a comparative analysis between LMC–SMC–MW, NGC 2718-UGC 4703, and NGC 2998 -MCG+07-20-052. We found that NGC 2998 is located in a relatively denser environment compared to the MW and NGC 2718. In addition, unlike the MS we do not detect any H I extension connecting MCG+07-20-052 and the host NGC 2998.

ORCID iDs

Sanjaya Paudel https://orcid.org/0000-0003-2922-6866
Suk-Jin Yoon https://orcid.org/0000-0002-1842-4325

References

Abazajian, K. N., Adelman-McCarthy, J. K., Agüeros, M. A., et al. 2009, ApJS, 182, 543
Abramson, A., Kenney, J. D. P., Crowl, H. H., et al. 2011, AJ, 141, 164
Barnes, J. E. 1992, ApJ, 393, 484
Bekki, K. 2008, MNRAS, 388, L10
Besla, G., Kallivayalil, N., Hernquist, L., et al. 2012, MNRAS, 421, 2109
Besla, G., Patton, D. R., Stierwalt, S., et al. 2018, MNRAS, 480, 3376
Blum, R. D., Burleigh, K., Dey, A., et al. 2016, AAS Meeting, 228, 317.01
Boylan-Kolchin, M., Springel, V., White, S. D. M., & Jenkins, A. 2010, MNRAS, 406, 896
Coleman, M., Da Costa, G. S., Bland-Hawthorn, J., et al. 2004, AJ, 127, 832
Davis, D. S., Keel, W. C., Mulchaey, J. S., & Henning, P. A. 1997, AJ, 114, 613
Deason, A., Wetzel, A., & Garrison-Kimmel, S. 2014, ApJ, 794, 115
Duc, P.-A., Cuillandre, J.-C., Karabal, E., et al. 2015, MNRAS, 446, 120
Duc, P.-A., Cuillandre, J.-C., Serra, P., et al. 2011, MNRAS, 417, 863
Elmegreen, D. M., Elmegreen, B. G., Sánchez Almeida, J., et al. 2012, ApJ, 750, 95
Fakhouri, O., Ma, C.-P., & Boylan-Kolchin, M. 2010, MNRAS, 406, 2267
Fitts, A., Boylan-Kolchin, M., Bullock, J. S., et al. 2018, MNRAS, 479, 319
Glatt, K., Grebel, E. K., & Koch, A. 2010, A&A, 517, A50
Harris, J., & Zaritsky, D. 2009, AJ, 138, 1243
Haynes, M. P., & Giovanelli, R. 1984, AJ, 89, 758
Kado-Fong, E., Greene, J. E., Greco, J. P., et al. 2020, AJ, 159, 103
Karachentsev, I. D., Makarov, D. I., & Kaisina, E. I. 2013, AJ, 145, 101
Kennicutt, R. C., Jr. 1998, ARA&A, 36, 189
Klimentowski, J., Łokas, E. L., Knebe, A., et al. 2010, MNRAS, 402, 1899
Lee, J. C., Kennicutt, R. C., Jr., Funes, S. J. J. G., Sakai, S., & Akiyama, S. 2009, ApJ, 692, 1305
Liu, L., Gerke, B. F., Wechsler, R. H., Behroozi, P. S., & Busha, M. T. 2011, ApJ, 733, 62
Marino, R. A., Rosales-Ortega, F. F., Sánchez, S. F., et al. 2013, A&A, 559, A114
Martin, D. C., Fanson, J., Schiminovich, D., et al. 2005, ApJL, 619, L1
Meyer, H. T., Lisker, T., Janz, J., & Papaderos, P. 2014, A&A, 562, A49
Mihos, J. C., & Hernquist, L. 1994, ApJL, 425, L13
Naab, T., & Ostriker, J. P. 2009, ApJ, 690, 1452
Noeske, K. G., Iglesias-Páramo, J., Vílchez, J. M., Papaderos, P., & Fricke, K. J. 2001, A&A, 371, 806
Paudel, S., & Sengupta, C. 2017, ApJL, 849, L28
Paudel, S., Sengupta, C., & Yoon, S.-J. 2018a, AJ, 156, 166
Paudel, S., Smith, R., Duc, P.-A., et al. 2017, ApJ, 834, 66
Paudel, S., Smith, R., Yoon, S. J., Calderón-Castillo, P., & Duc, P.-A. 2018b, ApJS, 237, 36
Pearson, S., Besla, G., Putman, M. E., et al. 2016, MNRAS, 459, 1827
Pearson, S., Privon, G. C., Besla, G., et al. 2018, MNRAS, 480, 3069
Privon, G. C., Stierwalt, S., Patton, D. R., et al. 2017, ApJ, 846, 74
Ramatsoku, M., Serra, P., Poggianti, B. M., et al. 2019, MNRAS, 487, 4580
Robotham, A. S. G., Baldry, I. K., Bland-Hawthorn, J., et al. 2012, MNRAS, 424, 1448
Salem, M., Besla, G., Bryan, G., et al. 2015, ApJ, 815, 77
Schlafly, E. F., & Finkbeiner, D. P. 2011, ApJ, 737, 103

Paudel et al.

Sengupta, C., Balasubramanyam, R., & Dwarakanath, K. S. 2007, MNRAS, 378, 137

Stierwalt, S., Besla, G., Patton, D., et al. 2015, ApJ, 805, 2

Tollerud, E. J., Boylan-Kolchin, M., Barton, E. J., Bullock, J. S., & Trinh, C. Q. 2011, ApJ, 738, 102

Tully, R. B., Courtois, H. M., & Sorce, J. G. 2016, AJ, 152, 50

Wilman, D. J., Fontanot, F., De Lucia, G., Erwin, P., & Monaco, P. 2013, MNRAS, 433, 2986

Zhang, H.-X., Puzia, T. H., & Weisz, D. R. 2017, ApJS, 233, 13